

TECHNICAL ADVANCE/RESOURCE

***In vivo* extraction of Arabidopsis cell turgor pressure using nanoindentation in conjunction with finite element modeling**

Elham Forouzes¹, Ashwani Goel¹, Sally A. Mackenzie² and Joseph A. Turner^{1,*}¹Department of Mechanical and Materials Engineering, University of Nebraska-Lincoln, W342 Nebraska Hall, Lincoln, NE 68588-0526, USA, and²Center for Plant Science Innovation, University of Nebraska-Lincoln, Lincoln, NE 68588-0660, USA

Received 9 November 2011; revised 26 September 2012; accepted 1 October 2012; published online 10 December 2012.

*For correspondence (e-mail jaturner@unl.edu).

SUMMARY

Turgor pressure in plant cells is involved in many important processes. Stable and normal turgor pressure is required for healthy growth of a plant, and changes in turgor pressure are indicative of changes taking place within the plant tissue. The ability to quantify the turgor pressure of plant cells *in vivo* would provide opportunities to understand better the process of pressure regulation within plants, especially when plant stress is considered, and to understand the role of turgor pressure in cellular signaling. Current experimental methods do not separate the influence of the turgor pressure from the effects associated with deformation of the cell wall when estimates of turgor pressure are made. In this paper, nanoindentation measurements are combined with finite element simulations to determine the turgor pressure of cells *in vivo* while explicitly separating the cell-wall properties from the turgor pressure effects. Quasi-static cyclic tests with variable depth form the basis of the measurements, while relaxation tests at low depth are used to determine the viscoelastic material properties of the cell wall. Turgor pressure is quantified using measurements on *Arabidopsis thaliana* under three pressure states (control, turgid and plasmolyzed) and at various stages of plant development. These measurements are performed on cells *in vivo* without causing damage to the cells, such that pressure changes may be studied for a variety of conditions to provide new insights into the biological response to plant stress conditions.

Keywords: nanoindentation, cell-wall measurement methods, viscoelastic properties, computational models, turgor pressure, technical advance.

INTRODUCTION

Plant cell walls are complex and dynamic structures composed mainly of a network of extended polysaccharides, providing structural support and protection to the cell (Somerville *et al.*, 2004). This structure acts as an effective pressure vessel for the plant, preventing over-expansion due to water uptake by osmosis (Gorshkova *et al.*, 2010). The thickness, rigidity and viscoelastic behavior of the cell wall determine the size, shape, morphology and growth behavior of a plant. These parameters also determine the behavior of the cell wall with respect to the hydrostatic pressure of the cell, commonly known as turgor pressure (Nobel, 2005). The typical turgor pressure in plants is in the range of 0.3–1.0 MPa, a value that translates to between 10 and 100 MPa of tensile stress in the walls (Wei and Lintilhac, 2007). It has been recognized that cell

enlargement occurs due to wall relaxation, a viscoelastic process that causes yielding of the matrix and allows the microfibrils to rearrange or move apart, leading to growth of the plant. Turgor pressure provides the driving force for the wall deformation that occurs as a result of such relaxation (Cosgrove, 2005). A recent study by Heisler *et al.* (2010) showed that morphogenesis during plant development is determined by intercellular signaling molecules as well as by the mechanical properties of individual cell walls. This process involves complex interactions between cell components such as the cell wall and cortical microtubules (Allard *et al.*, 2010a,b; Zhang *et al.*, 2011). The microtubules are greatly influenced by the strain on the cell wall caused by the stress differential across the wall (Hamant *et al.*, 2011). The origin of this stress on the cell

wall is the turgor pressure inside the cell. Therefore, turgor pressure, in association with altered mechanical properties of the cell wall, may be involved in cell-to-cell signaling and growth responses, as well as coordination between growth direction and growth magnitude (Ache *et al.*, 2010; Heisler *et al.*, 2010; Hamant *et al.*, 2011; Shi *et al.*, 2011). To understand these cellular properties, it is important for scientists to be able to quantify the turgor pressure of cells, as well as the corresponding wall stress values, especially with respect to any *in vivo* changes that may occur due to biological or environmental effects.

Mean turgor pressure may be determined from measurements on entire leaves using tools such as thermocouple psychrometers and pressure chambers (Mokter and Nonami, 2010) or from ultrasonic spectroscopy measurements (Sancho-Knapik *et al.*, 2010). These methods quantify the water status of a given tissue but cannot be used to study single cells. Measurement of pressure in single cells was first performed using a pressure probe (Green and Stanton, 1967), in which a pipette is used to puncture the cell wall while the pressure in the pipette is monitored. This technique, which measures pressure in a direct manner, is now the conventional method for measuring turgor pressure in single cells. However, the pressure probe has its own limitations. First, it is a destructive test that requires the cell wall to be punctured, so it is difficult to quantify biological or environmental effects that influence turgor pressure in a particular cell. Second, it is difficult to apply this procedure to very small cells because the volume of sap entering the pipette must be much smaller than the total cell volume to allow the cell to reach equilibrium after insertion of the probe (Green and Stanton, 1967). Otherwise, measurement errors will be too large. Later methods were developed to quantify the turgor pressure of a single cell non-destructively by applying a compression load to the cell and monitoring the contact area with a microscope (Lintilhac *et al.*, 2000; Wang *et al.*, 2006). Lintilhac *et al.* (2000) used a glass ball to apply a load to the surface of onion cells. The projected area of the contact patch was captured by video microscopy. From the load and projected area, the pressure was estimated assuming a balance between the load and pressure (i.e. it was assumed that the cell wall does not support the load). Wang *et al.* (2006) compared the value obtained for turgor pressure in a single tomato cell using a pressure probe and a compression load applied using micro-manipulation. Although such procedures are in principle applicable at any scale, their use on small cells such as those of Arabidopsis is not practical because the contact patch is too small to measure via optical microscopy. In this study, a method is developed that uses nanoindentation to quantify turgor pressure *in vivo* in Arabidopsis leaf epidermis cells. The technique is similar to that described by Lintilhac *et al.* (2000) because it involves a tip in contact with the cell wall.

A recent study by Routier-Kierzkowska *et al.* (2012) also involved use of a tip to deform the cell walls of onion cells. They used finite element simulations to interpret their results and to examine the behavior of cells as they recover from plasmolysis. Here, the tip is small enough that measurements on Arabidopsis cells are not difficult. In addition, the loads are small enough that the influence of the cell wall must be included in the analysis because the wall's resistance to shear and bending loads is important.

Nanoindentation has proven itself to be a powerful technique for measurement of mechanical properties in diverse biomaterials ranging from mineralized tissues to soft tissues (Ebenstein and Pruitt, 2004; Hoffler *et al.*, 2005; Ebenstein *et al.*, 2008). This technique has a high spatial resolution due to the small tip diameter. Quasi-static and dynamic tests may be performed on samples so that elastic and viscoelastic properties may be determined (Fischer-Cripps, 2002). From the load displacement data, mechanical properties such as hardness and elastic modulus may be determined (Johnson, 1985). Such measurements may also be obtained as a function of time, such that the viscoelastic behavior of a sample may be quantified. A commonly used method to characterize viscoelastic properties is the relaxation test, in which the indenter is kept at a constant indentation depth and the changing load is recorded over time (Yuya *et al.*, 2010). Another method, the dynamic nanoindentation technique, uses a small sinusoidal force that is superimposed with the applied quasi-static force to the indenter (Zhang *et al.*, 2008). The dynamic nanoindentation method was recently used to quantify the viscoelastic properties of plant cell walls *in vivo* (Hayot *et al.*, 2012).

In this paper, nanoindentation measurements are combined with finite element simulations to determine the turgor pressure of Arabidopsis cells *in vivo*. Quasi-static cyclic tests with variable depth form the basis for the measurements, and relaxation tests are used to determine the viscoelastic material properties of the cell wall. We hypothesize that low-depth measurements will be most sensitive to the cell-wall properties, while large-depth measurements will be most sensitive to the turgor pressure. This hypothesis is based on similar behavior associated with thin films deposited on substrates. As shown by others (Tsui and Pharr, 1999; Saha and Nix, 2002; Tricoteaux *et al.*, 2010), low-depth indentations on thin films may be used to extract properties of the films. However, when the indentation depth is beyond a certain depth, the measurements are influenced greatly by the substrate properties. In our study, the response of the pressurized cell is analogous to the thin film problem, in which the cell wall plays the role of the film and the pressure boundary condition is analogous to the substrate: once the depth is large enough, the turgor pressure will influence the measurements. Therefore, a cyclic depth-dependent measurement will include the response of all important components.

RESULTS

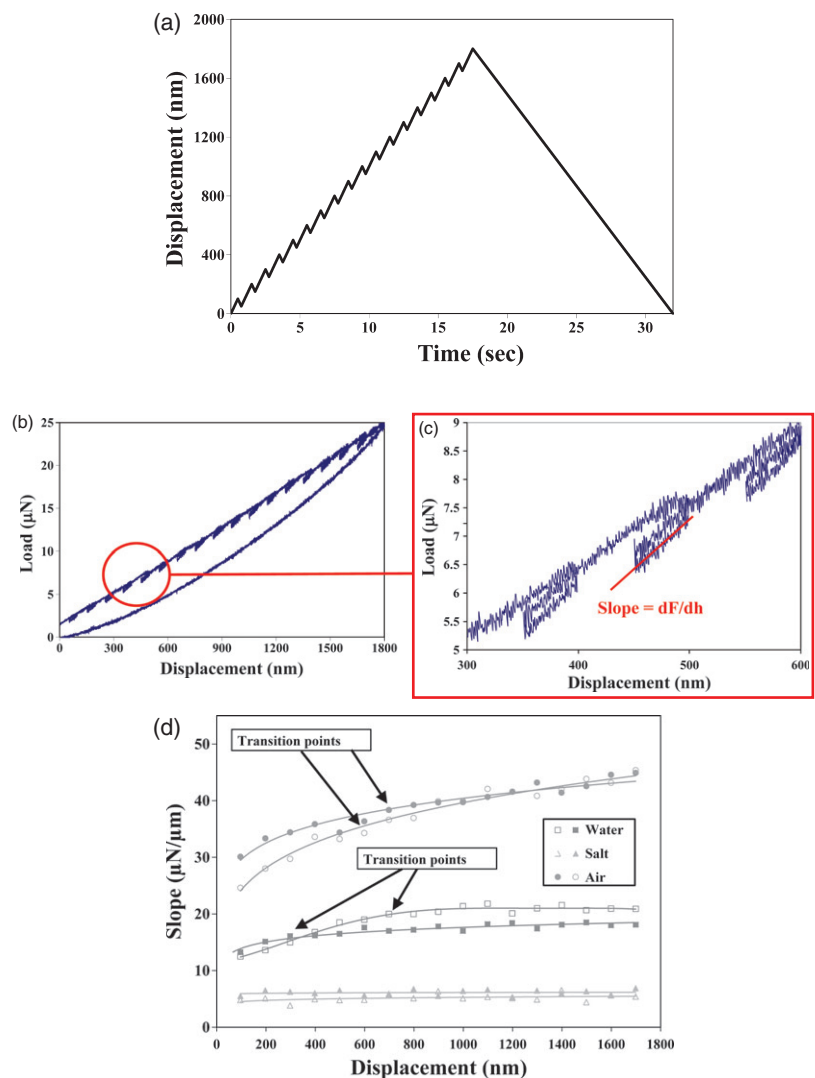
In this study, initial nanoindentation experiments were performed in quasi-static mode using a spherical tip with 2.5 μm radius (so that the tip geometry is known). Feedback control testing, in displacement-controlled mode, provided precise control of the tip location with respect to the sample. The tip was first engaged with the sample to a prescribed initial load (here 2 μN). A displacement control function (displacement–time curve) was then defined for the tip motion during the experiment. The actual tip displacement and applied force were then recorded during testing. Such measurements generate a load–displacement curve from which sample properties may be determined. If such measurements are performed on homogeneous samples (which are large relative to the contact area; the sample is effectively a half space), the load–displacement curve may be used to extract the sample modulus using the

slope of the unloading portion of the curve and contact area, assuming a linear elastic response (Oliver and Pharr, 2004). The sample here is much more complicated, as effects from the cell-wall properties as well as the turgor pressure must be included in the analysis as described above. These concepts led to the experiment design: a displacement profile is used with small unloading segments at various depths from which the slope at a given depth may be determined. Because cell-wall properties and turgor pressure influence all measurements to some degree, a computational model was necessary to separate these effects.

The measurement protocols were developed by performing several such depth-dependent tests. Figure 1(a) shows the displacement–time curve used, which includes a complete loading/unloading profile with several small unloading segments. The tests were performed at a constant depth rate of 200 nm/sec, with 150 nm loading and

Figure 1. Nanoindentation load function, a resulting load–displacement curve, and sample slope–displacement measurements.

(a) Prescribed displacement–time curve input to the experiments.
 (b) Measured load–displacement curve obtained from cyclic nanoindentation.
 (c) Slope determination from the unloading portion of the curve.
 (d) Slope–displacement curves obtained from the nanoindentation cyclic tests performed under various conditions: in air (control sample), in salt (plasmolyzed sample) and in water (turgid sample). The arrows show the transition points at a certain depth after which the slope remains constant.



50 nm unloading in each increment. Figure 1(b) shows the force–displacement response from an Arabidopsis cell resulting from the defined input cycle. From the force–displacement data at each depth, the slope (dF/dh) was calculated from the unloading section using a linear fit as shown in Figure 1(c).

In order to identify the influence of pressure change on the measurements, a cyclic nanoindentation experiment was performed on Arabidopsis cell walls under three environmental conditions; turgid (sample in water), plasmolyzed (sample in salt solution) and control (sample in air). More than 40 measurements were performed for each environmental condition. The slope–displacement curves of two such measurements for each case are shown in Figure 1(d). The data show that there is a clear difference in slope with cell environment: lowest for plasmolyzed, intermediate for control, and highest for turgid samples. Because these samples differ primarily in their turgor pressure, it is expected that the slope is related to the pressure. These initial results showed the sensitivity of the measurement with respect to the changing cell environment, and provide insight into the computational model required to extract turgor pressure.

There is another important feature in the measurements shown in Figure 1(d) that is unlike the response observed in half-space samples for which the slope increases with depth (Frommer and Overney, 2000). For plant cells, the slope increases until a certain depth (shown as a transition point in Figure 1d), and then tends toward an asymptotic value. This transition point varies slightly with measurement position, but is influenced greatly by the cell environment: more turgid samples have deeper transition points while the plasmolyzed sample does not show a clear transition point (see Supporting information, Figure S5).

To understand the measurements and to extract quantitative information from the data, computational simula-

tions were created to model the indentation experiments (see Supporting information and Figure S1 for details). An example of a simulated indentation is shown in Figure 2. Subsequently, the method was applied to samples at various developmental stages to test the ability of the method to extract biological changes associated with development from the measurements.

Quantification of cell turgor pressure

Quantification of single-cell turgor pressure required a computational model for interpretation of the depth-dependent nanoindentation measurements. In addition to the unknown turgor pressure, several other parameters were needed (see Figure S1). These unknowns include the viscoelastic material properties (E_1/E_0 and τ_1), the thickness of the cell wall, and the instantaneous elastic modulus E_0 . First, low-depth relaxation tests were used to determine the viscoelastic material parameters for entry into the computational model. Simulations of the depth-dependent cyclic tests were then used to relate the transition points (Figure 1d) of the experimental depth-dependent slopes to the cell-wall thickness (another model input). Finally, the computational model was used iteratively to determine the instantaneous elastic modulus and turgor pressure. Each of these steps is described in detail below.

Viscoelastic properties

The relaxation tests (see Supporting information) were performed at 500 nm depth. Each sample was indented using a displacement-controlled ramp function with 100 nm sec^{-1} loading, 500 nm peak displacement with a holding period of 40 sec, and then 100 nm sec^{-1} unloading. Multiple indents (seven or eight) were performed on the sample, and the force was recorded as a function of time for each measurement. A normalized force versus time plot

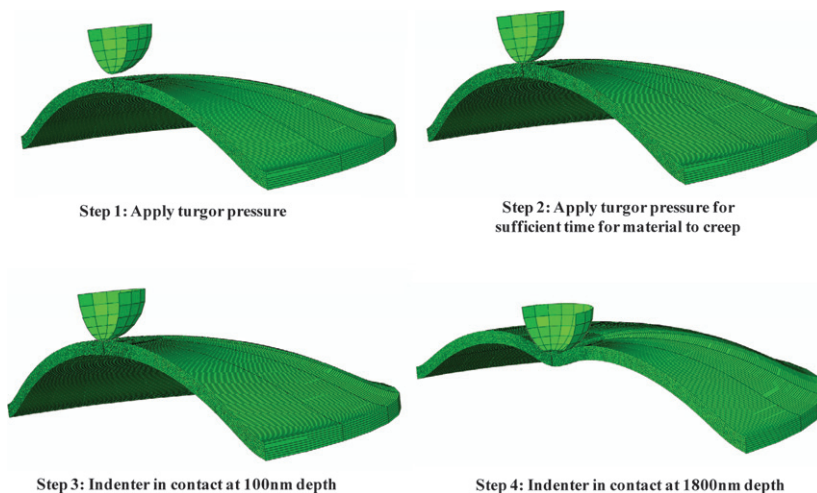


Figure 2. Steps used in performing the finite element simulation.

Note that the model is actually axisymmetric, but these images provide a clearer representation of the steps used for the simulations and the relative degree of deformation during indentation.

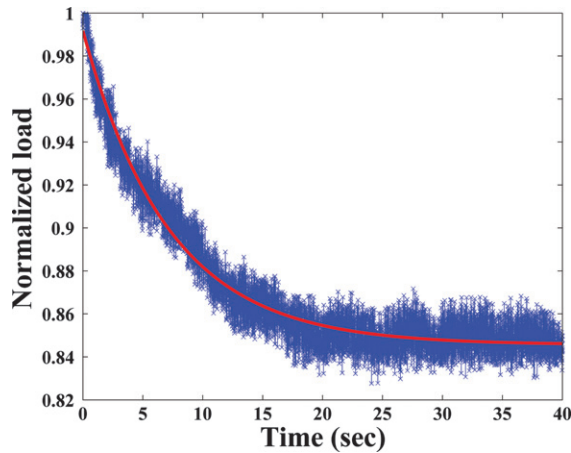


Figure 3. Normalized load versus time plot for a typical relaxation test to determine relaxation time.

The solid line is a theoretical curve fitted to the experimental data Eq. (S2) (see Method S1).

for one such experiment is shown in Figure 3 (performed on a 22-day-old sample). The parameters E_1/E_0 and τ_1 were calculated from the experimental data by fitting the hold section of the normalized load versus time plot for all the relaxation experiments performed (see Supporting information). The solid line in Figure 3 is the curve fit for the data shown.

Cell-wall thickness. The initial experimental results shown in Figure 1(d) indicate a distinct transition point in the slope versus depth curve. To understand the role of wall thickness on the transition point, numerous simulations were performed. Some of these results are shown in Figure 4, covering a range of thickness from 0.6–1.5 μm , a range of instantaneous modulus from 75–150 MPa, and a range of turgor pressure from 0.1–0.4 MPa. These results show that the transition depth is highly correlated with thickness. From our simulations, we conclude that the cell-wall thickness is approximately 1.8 times the transition depth. The cell-wall thickness was calculated for each experimental slope versus depth curve using the prescribed method by fitting a third-order polynomial to the experimental slope versus depth curve. The transition point was selected at the position at which the change in slope with an increase in depth was less than 2% (implying that the asymptotic value at large depth had been achieved). The thickness was then calculated from this transition value.

Turgor pressure and instantaneous elastic modulus. The two parameters that remain to be determined are the instantaneous elastic modulus of the cell wall (E_0) and the turgor pressure. Our simulations confirmed our hypothesis that the slope at low depth was most sensitive

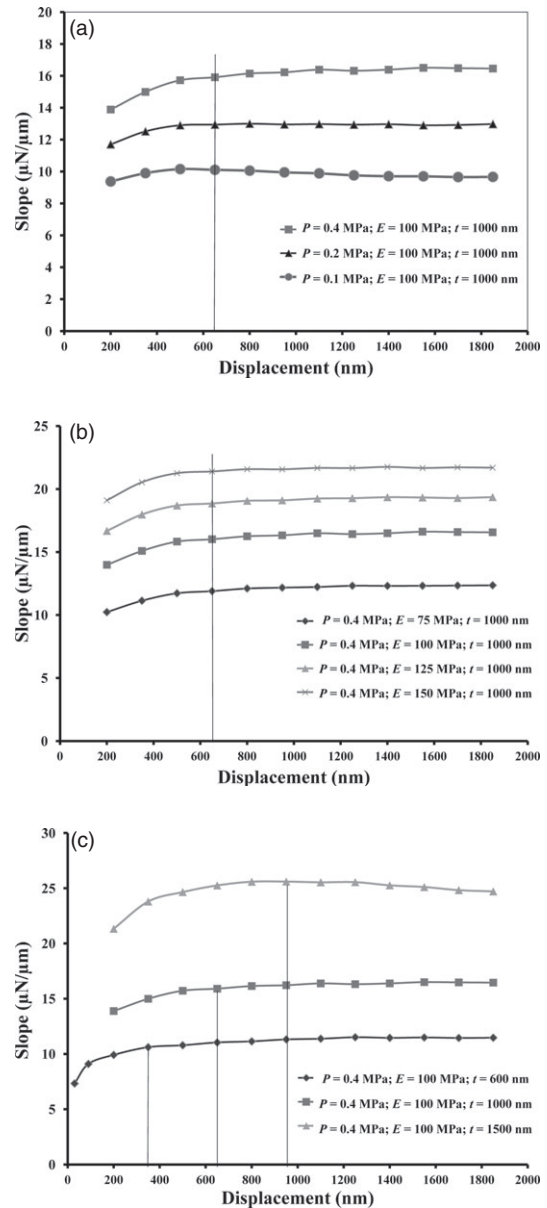


Figure 4. Slope–displacement plot for cyclic tests from finite element simulations.

(a) The cell-wall thickness and instantaneous elastic modulus are kept constant at 1000 nm and 100 MPa, respectively, and the turgor pressure is changed.

(b) The cell-wall thickness and turgor pressure are kept constant at 1000 nm and 0.4 MPa, respectively, and the instantaneous elastic modulus is changed.

(c) The turgor pressure and instantaneous elastic modulus are kept constant at 0.4 and 100 MPa, respectively, and the cell-wall thickness is changed. The perpendicular lines in all three graphs indicate the transition points in slope–displacement curves that are related to the cell-wall thickness.

to the cell-wall properties (and therefore E_0), more so than to the turgor pressure. In contrast, the slope at large depth was most sensitive to the turgor pressure. Thus, for each slope versus displacement curve obtained from the cyclic nanoindentation experiments, an iterative fitting procedure

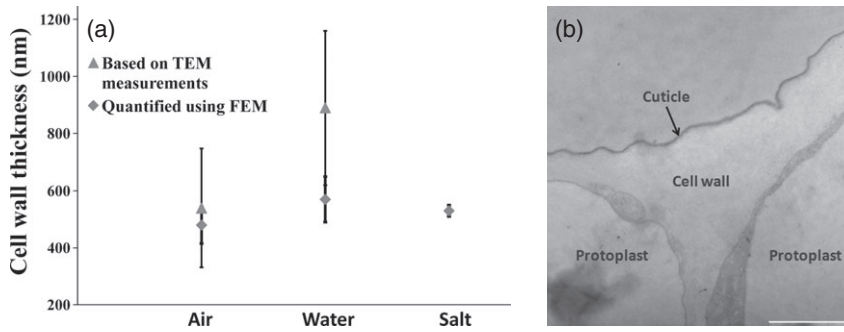


Figure 5. Cell-wall thickness estimates. (a) Estimates of the cell-wall thickness using our combined measurement and modeling procedure for specimens tested in air and water compared with the values obtained from TEM observations (error bars represent the standard deviation of the results). (b) TEM image of a Col-0 cell wall (transverse section). The cell wall has a non-uniform thickness, especially at the interface of adjacent cells. Scale bar = 1 μm.

was used to find these values by matching the initial and final slopes from each experimental curve. First, the turgor pressure was assumed to be 1 MPa (although we found that the initial guess of the turgor pressure was not particularly important). Then the simulation was repeated several times with different values of E_0 until the simulation matched the experimental value of slope at the lowest depth, 100 nm. This value of E_0 was then used for simulations with varying turgor pressure in order to match the slope at large depth. This process was repeated until the values for E_0 and turgor pressure from successive simulations change by less than 1%. In all cases, it usually took five or six iterations for the procedure to converge. This procedure to extract thickness, instantaneous elastic modulus and turgor pressure was used for two important examples: the first associated with plasmolysis and the second associated with plant age.

Effect of plasmolysis

The first set of experiments used 22-day-old Col-0 and involved three environmental states associated with the leaf in air, water and salt solution (see Experimental procedures). The viscoelastic material parameters obtained from the fit of relaxation experiments are $E_1/E_0 = 0.225 \pm 0.063$ (note that this parameter is dimensionless) and $\tau_1 = 7.44 \pm 3.2$ sec. Thickness results, obtained using the method described above, for all three environmental conditions are shown in Figure 5(a). The uncertainty shown reflects the fact that the thickness at each measurement position may be different. Because it is not possible to measure thickness exactly at the indentation point, transmission electron microscopy (TEM) was used to corroborate the thickness values obtained for the cells in air (Figure 5b). In general, the cell wall is thinnest in the center of the cell and thickest near the anticlinal walls. Thickness values obtained from the TEM image are also shown in Figure 5(a), with reasonable agreement with thickness results obtained from the measured transition point. Plasmolyzed samples, on the other hand, do not show a clear transition point in the slope versus depth curve. A transition may exist below 200 nm. Unfortunately, measurements at depths below 100 nm are not

accurate for these samples due to surface/adhesion effects (see Supporting information). Therefore, the cell-wall thickness in subsequent simulations for the plasmolyzed samples was examined over a range of 250–350 nm.

The resulting values of instantaneous elastic modulus and turgor pressure determined using this method are shown in Figure 6(a,b) for the three sets of samples (plasmolyzed, control and turgid) for which two different

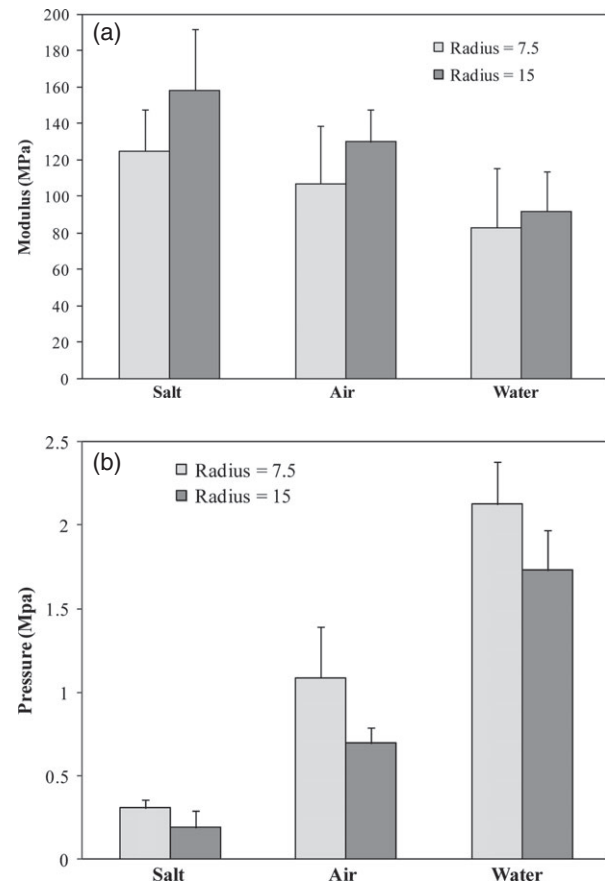


Figure 6. Results calculated from fitting the experimental slope values using finite element simulations for the samples tested in salt, air and water. (a) Elastic modulus. (b) Turgor pressure. Error bars represent the standard deviation of the results.

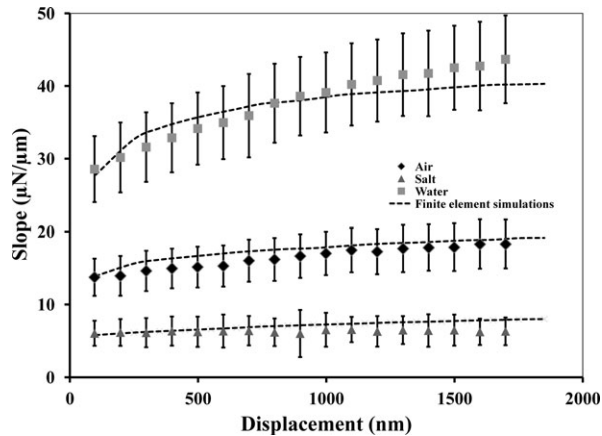


Figure 7. Slope–displacement curves obtained from nanoindentation cyclic tests under three different conditions, and a comparison of them with finite element simulations.

Error bars represent the standard deviation of the results.

cell radii were used in the analysis. The instantaneous elastic modulus values (Figure 6a) are maximum for the plasmolyzed samples and minimum for turgid samples. The mean instantaneous elastic moduli (cell radius $R = 7.5 \mu\text{m}$) for plasmolyzed, normal and turgid environments are 124 ± 22 , 106 ± 31 and 79 ± 25 MPa, respectively. There is no significant difference ($P > 0.05$) between the modulus results for cells of different radii ($R = 7.5$ and $15 \mu\text{m}$). The difference between the modulus values for control and plasmolyzed samples is also negligible ($P > 0.05$). However, the turgid samples show a lower modulus compared with the plasmolyzed and control samples ($P < 0.05$).

Figure 6(b) summarizes the values obtained for the turgor pressure of the samples. The mean turgor pressures ($R = 7.5 \mu\text{m}$) estimated for the plasmolyzed, normal and turgid environments are 0.31 ± 0.050 , 1.1 ± 0.30 and 2.1 ± 0.26 MPa, respectively. The turgor pressure values determined when a larger radius was used in the model ($R = 15 \mu\text{m}$) were 0.19 ± 0.19 , 0.69 ± 0.18 and 1.7 ± 0.48 MPa for the plasmolyzed, normal and turgid samples, respectively. Statistical analysis for the turgor pressure results shows that the radius of the cell used in the model has a greater impact on the final turgor pressure estimates than it has for the values of modulus, i.e. turgor pressure values using the measurement/simulation approach

described here for a cell with radius $R = 7.5 \mu\text{m}$ are statistically different from the results obtained using a cell with $R = 15 \mu\text{m}$ ($P < 0.005$).

Simulation results for the slope are shown in Figure 7 for the three cases using mean values found from the combined measurement/simulation ($R = 15 \mu\text{m}$). The results obtained from the simulations match reasonably well with the experimental results for each of the environmental conditions.

Effect of age

Our approach was also applied to leaves at various stages of development in the control environmental state (i.e. air). Cell size was determined using confocal microscopy with image analysis software (see Experimental procedures). Relaxation tests were then used to determine the visco-elastic properties of the cell wall. Finally, the depth-dependent measurements were used with the computational model to determine the cell-wall thickness, cell-wall modulus and turgor pressure.

Table 1 summarizes the results obtained for the cell size and for relaxation tests on samples at each age investigated. According to the results, 12-day-old plant samples show a higher value of E_1/E_0 compared with older plants (22–32 days old). This result indicates a decrease in the viscous behavior of the cell wall with age. This phenomenon is also confirmed in the relaxation time results. (Note: the values reported for the 22-day-old sample in this set of results are statistically the same as those for samples for which the effect of plasmolysis was reported earlier; $P > 0.05$). Clearly, the relaxation time of the cell wall reduces with age, meaning that a young wall is more viscous and therefore takes a longer time to relax to a specific load, while an older wall will relax sooner. For samples at senescence, the properties are more complicated. It is at this stage of development that the cell wall begins to lose its integrity. The results shown in Table 1 support this understanding of the cell-wall breakdown, and provide quantitative information about the size of the change with respect to the mechanical response.

The cyclic depth-dependent nanoindentation method was also used on these samples. Cell-wall thickness, cell-wall modulus and turgor pressure were quantified as described above. Results for the cell-wall instantaneous modulus with respect to age do not show statistically significant differences for any age ($P > 0.05$; $E_0 = 65.9$

Table 1 Results from the age-related study for the cell radius, as well as the relaxation test results for E_1/E_0 and relaxation time (τ_1)

	12 days old	22 days old	32 days old	Senescence
Cell radius (μm)	7.5 ± 1	10 ± 0.9	12 ± 0.6	12.5 ± 0.5
E_1/E_0	0.316 ± 0.0781	0.254 ± 0.0736	0.155 ± 0.0195	1.93 ± 0.631
Relaxation time (sec)	12.9 ± 1.54	6.88 ± 2.09	4.88 ± 1.15	23.5 ± 5.02

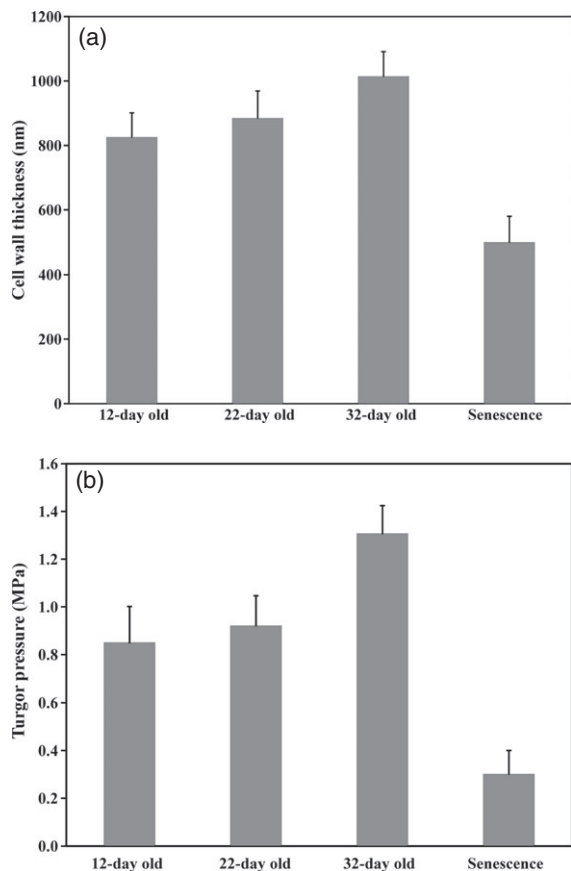


Figure 8. Results obtained for the samples tested in air as a function of age using the combined measurement and modeling procedure described in the text.

(a) Cell-wall thickness.

(b) Cell turgor pressure. Error bars represent the standard deviation of the results.

± 14.1 MPa). Although there is a decrease in the viscosity of the mature samples (Table 1), the instantaneous modulus is not affected. The results for thickness and turgor pressure are shown in Figure 8(a,b). The change in cell-wall thickness for the 12- and 22-day-old samples was not statistically different ($P > 0.05$) (Figure 8a). However, samples from the 32-day-old mature plants showed a statistically significant increase in cell-wall thickness ($P < 0.05$). In the senescing samples (52 days old), there was a very large decrease in cell-wall thickness, in agreement with knowledge regarding cell-wall breakdown during senescence. The results for turgor pressure, shown in Figure 8(b), indicate that the turgor pressure increases with age up to the maturation stage. However, at senescence, the cells show a dramatic reduction in turgor pressure.

DISCUSSION

Using the nanoindentation technique described here, in conjunction with finite element modeling, the turgor pres-

sure, cell-wall thickness and elastic modulus have been quantified in living plant cells. In order to demonstrate that this technique captures differences in cell turgor pressure, cell-wall thickness and cell-wall elastic modulus, samples were prepared under three environmental conditions (turgid, control and plasmolyzed). Furthermore, to demonstrate an important application of this method in biology, the above parameters were quantified for plants at various developmental stages.

The results showed that the thickness values quantified by this method are in the range measured by other methods for Col-0 (Derbyshire *et al.*, 2007, Conn *et al.*, 2011). The results shown in Figure 5 suggest that the cell-wall thickness is also affected by the environment – the cell wall is dynamic and responds to the environmental changes. In a high-humidity environment, water passes through the wall and makes the cell turgid by osmosis. Some of this water is trapped inside the wall, leading to swelling of the cell wall and increasing its thickness. A similar observation was made by Niklas (1992) with respect to collenchyma cells, in which the cell-wall thickness for tissue immersed in water was shown to increase by as much as 150% compared with the cell-wall thickness for the same tissue in air. Similarly, there is an expectation that plasmolyzed samples will show a decrease in thickness. Unfortunately, the nanoindentation measurements were not accurate for shallow depths, so that the wall thickness for plasmolyzed samples may only be estimated as less than 200 nm.

The measured values of slope (examples given in Figure 1d) are in the range of values measured by Rottier-Kierzkowska *et al.* (2012) on onion cells over a wide range of turgor pressure as the cells recovered from plasmolysis. In our study, the elastic modulus of the cell wall was determined using finite element simulations to match the experimental slope results. The moduli results for control and plasmolyzed cells were very similar, but the turgid sample showed a lower elastic modulus. This result suggests that the cell wall of a sample kept in water may change more dramatically than that of a sample held in a plasmolyzing solution. However, these findings should be further investigated using other techniques before any stronger conclusions may be drawn. The cell-wall modulus was quantified at a much smaller length scale by Milani *et al.* (2011) using an atomic force microscope. They reported that the cell wall has the same modulus in both water and salt solutions. However, it should be noted that the tip radius associated with their measurements is much smaller than that used here, highlighting the multiple length scales associated with the structure of the cell wall. Values for the elastic modulus of plant cell walls in the literature range from hundreds of MPa to a few GPa. Wang *et al.* (2004) and Bolduc *et al.* (2006) considered 185 MPa as the value of modulus in their simulations. Cell wall

moduli have also been measured in Characeae, and the results show that moduli may vary widely, even in closely related plants. The modulus of the cell wall was measured in *Chara corallina* (Wei and Lintilhac, 2007) as a function of age, and was found to be 213 MPa for young samples and 361 MPa for older samples. Probine and Preston (1962) reported modulus values of 450–1000 MPa for *Nitella opaca*. An upper limit for cellulose microfibrils of 145 GPa is also given in some studies (Iwamoto S. and Isogai A., 2009). However, because most of these studies do not indicate the loading rate used in the experiments, it is difficult to make careful comparisons for time-dependent (viscoelastic) materials.

The values determined for the turgor pressure of the plant cells under various environmental conditions were in agreement with the results reported by Inan *et al.* (2004). As expected, maintaining the plant in water causes the cells to absorb water osmotically through the wall, forming turgid cells. Thus, the turgor pressure obtained for the cells kept in water was higher compared with the samples kept in air. On the other hand, plasmolysis causes osmotic water loss from cells, such that the turgor pressure decreases compared to the samples tested in air. These trends were captured very well using the method described.

The results associated with plant age are also in agreement with those of other researchers. Abarca *et al.* (2001) reported that the rate of growth was smallest for the youngest plants, suggesting that the expansibility of the cell wall changes with age. Also, Derbyshire *et al.* (2007) reported that, with age, there is a change in the degree of methyl esterification, which plays an *in vivo* mechanical role within the cell. The degree of methyl esterification is defined as the percentage of methyl-esterified carboxyl groups (-COOMe) on homogalacturonan molecules in pectin polysaccharide. This esterification blocks cross-linking by removing the negative charge from the carboxylate ion. A lower degree of methyl esterification leads to a less viscoelastic wall matrix, which reduces the wall relaxation in mature cells. This phenomenon occurs in concert with cessation of growth hormone secretion. It was reported by Goldberg *et al.* (1986) that mature cell walls have a lower degree of methyl esterification. These biological facts are in agreement with our results, which show that the relaxation time of the cell wall reduces with age (Table 1), implying that the cell wall in a young cell is more viscous than a mature wall. In a senescing cell, because photosynthesis has ceased, the cell is utilizing sugars in the wall (Mohapatra *et al.*, 2010), and the cell wall begins to lose its integrity and structural support.

Typically, the stretching due to growth increases the cell size by 10–100 times. However, it has been reported that the cell-wall thickness does not change during this process (Bret-Harte *et al.*, 1991). Thinning to the point of mechani-

cal instability is prevented by introduction of new material into the cell wall. However, although the cell no longer expands in mature cells, cell-wall components continue to be introduced into the wall, leading to an increase in cell-wall thickness (Wei and Lintilhac, 2007). In samples from senescing tissue, the cell walls serve as a source of nutrients for the cell and start to thin (Mohapatra *et al.*, 2010). The results obtained using our approach (Figure 8a) match these observations.

The change in the turgor pressure of cells with age has been confirmed previously (Zur *et al.*, 1981; Zhu and Boyer, 1992). When transpiration is negligible, water potentials in growing tissues are lower than in mature tissues. Such gradients move water into the enlarging cells. Because these cells have extensible cell walls, transport of water into these cells leads to irreversible growth of the tissue. It has also been reported (Nonami and Boyer, 1993) that the osmotic potential in a growing tissue is lower than in mature tissue. Under steady-state conditions, the pressure potential (ψ_p) is the difference between the water potential (ψ_w) and the osmotic potential (ψ_s), i.e. $\psi_p = \psi_w - \psi_s$. Therefore, the turgor pressure in mature cells is expected to be larger when compared with younger cells. During senescence, cells show a large reduction in turgor pressure that is attributable to the fact that cells are preparing for programmed cell death. The results obtained from the measurements in this study (Figure 8b) are in agreement with these biological expectations (Shibuya *et al.*, 2009; Das *et al.*, 2010).

Although these measurements show great promise with respect to quantitative measurements on living plant cells, future work must address issues associated with the tip position relative to the cell geometry. An improved optical microscope would allow precise positioning of the tip such that these effects may be accurately quantified. In addition, other important components of the cell, such as microtubules, may directly or indirectly influence the cell-wall mechanical response and should be included in future models. Finally, it is important to note that the turgor pressure results reported here were obtained indirectly through use of the computational model. As improved models are implemented, the accuracy of the pressure estimates is expected to improve as well.

EXPERIMENTAL PROCEDURES

Plant material and growth conditions

Arabidopsis thaliana (Col-0) seeds were stratified at 4°C for 2 days and then grown in a growth chamber for 22 days under 12 h day length at 24°C and relative humidity of 50–60%. Rosette leaves were numbered by emergence, reflecting their age, as shown in Figure S2.

Nanoindentation

Nanoindentation experiments were performed using a commercial TriboScope (Hysitron Inc). The indentations were performed using

a spherical indenter of radius 2.5 μm . To avoid dehydration of the samples and any change in the mechanical properties of the cell wall, all tests were performed on leaves attached to the plant. For consistency, tests were performed on leaf 3 of plants (22 days old unless otherwise stated), as shown in Figure S2. Nanoindentation was performed on cells from within the same area of the abaxial (lower) side of the leaf. The leaves were mounted to a sample holder disk using double-sided tape to eliminate any movement while performing the indentations. To ensure reproducibility of the results, 25 tests were performed on leaves from five plants.

The resolution of the nanoindenter camera was not sufficient to distinguish individual cells. Therefore, it was not possible to position the tip within single cells accurately. Thus, some of the nano-indentations may have been performed on the anticlinal walls or near guard cells. The possibility of coming into contact with such undesirable areas was estimated by Hayot *et al.* (2012) to be approximately 15–20% (Figure S3). However, measurements on undesirable regions were expected to look very different when compared with measurements near the middle of cells. For example, an indentation on an anticlinal wall was expected to show higher stiffness (due to the large wall depth) and was not expected to show an effect of pressure. Thus, the majority of the measurements that showed similar behavior were expected to come from positions away from anticlinal walls near the middle of the cells.

Sample preparation

To test the reliability of the method for determining turgor pressure, 22-day-old plant cells with various turgor pressures were prepared. Hypertonic samples were prepared by immersion of the leaves in 10% NaCl solution, and hypotonic samples were prepared by immersion of the leaves in pure water. The results for these two samples were compared with those for control cells tested in air.

In order to study the effect of age, four sets of Col-0 samples were grown to four developmental stages: 12, 22, 32 and 52 days (senescence). The cell size for each developmental stage was estimated from optical micrographs using ImageJ software (see below). The measured cell radii were 7.5 ± 1.0 , 10 ± 0.9 , 12 ± 0.6 and $12.5 \pm 0.5 \mu\text{m}$ for the 12-, 22-, 32- and 52-day-old samples, respectively.

Transmission electron microscopy

TEM images of cell walls were prepared as described by Pappozzi (1981). According to this protocol, sections of the leaf were cut and immediately immersed in fixative at 0–4°C (in ice). The fixative contained 1.5% para-formaldehyde/3% glutaraldehyde in 0.1 M sodium cacodylate, pH 7.0, plus 5 mg/ml CaCl_2 . Samples were fixed for 1 h. Samples were then post fixed (at 0–4°C) in 2% OsO_4 in 0.1 M sodium cacodylate, pH 7.0, overnight. Samples were then dehydrated and infiltrated. Transverse sections of three leaves per sample were observed at 30 kV using a Hitachi H7500 TEM with a Windows95/NT-based computerized operating system (Microsoft) for ultra-structural analysis of sections. Images were captured for many sections of each leaf, including regions near the anticlinal walls and regions between two anticlinal walls. Overall, a total of more than 150 images were analyzed. Wall thickness was determined by drawing a tangent to the outer side of the cell wall and measuring the amount of cell-wall material perpendicular to the tangent. The thickness of the cell wall was estimated at ten locations on each image. The values shown in Figure 5(a) represent the mean of at least 100 measurements.

Statistical analysis

A two-tailed paired Student's *t*-test was applied to the results to quantify the significance of the changes in stiffness with respect to the frequency as well as the significance of the stiffness changes with respect to the age of the leaf sample and genetic variation for specific frequencies. Each data point is given within a confidence level of 95%.

Image analysis and cell size measurements

To determine the approximate cell size for implementation in the finite element model, ImageJ 1.41o analysis software was used. The analysis was performed for plants of various ages: 12, 22, 32 and 52 days (senescence). For this purpose, the leaves were stained with fluorescent brightener 28 (F3543 Sigma-Aldrich), which binds to cellulose in the cell wall so that the cell wall is visible under a confocal microscope (Olympus FluoView 500 mounted on an Olympus BX60 compound microscope). This dye fluoresces (peak emission wavelength 450 nm) when excited with UV or near-UV light (optimum excitation wavelength 347 nm). The size of the cell was determined by drawing circles within the lobes of the cells. First the confocal image scale was defined in the software using the known micron/pixel values (Analyze→Set Scale). Then, using the circle drawing tool, a circle was drawn such that it fitted inside the cell. Finally, the area of the circle was measured using Analyze→Measure, from which the radii were determined (see Figure S4). This method was repeated 70 times on each image with three images used for each sample. Then the mean and standard deviation were calculated.

Image analysis and positional probability

Image analysis was performed on confocal images of leaves stained with fluorescent brightener 28 in order to determine the probability that the nanoindenter tip makes contact with anticlinal walls or guard cells (undesired regions). The undesired area was assessed by measuring the ratio of the area of the cell wall and guard cells to the whole area using ImageJ analysis software and a protocol modified from that described by Straatmann (2008). First the image scale was set using the known micron/pixel values (Analyze→Set Scale). Next the brightness and contrast was adjusted using the Image→Adjust brightness, contrast. Then the image was inverted using Edit→Invert, followed by Process→Make Binary to change the image to a binary format. The guard cells and anticlinal walls were filled in black using a paintbrush tool. Finally, the undesired area percentage (black to white ratio) was quantified using the Analyze→Measure tool. Figure S3 shows the images prepared at each of these steps.

ACKNOWLEDGEMENTS

This work was supported by the US National Science Foundation under grant number EPS-0701892 and by the Nebraska Center for Energy Sciences Research at the University of Nebraska-Lincoln.

SUPPORTING INFORMATION

Additional Supporting Information may be found in the online version of this article.

Figure S1. Finite element axisymmetric model for a plant cell wall subjected to turgor pressure and indentation load.

Figure S2. Leaf numbering in the rosette of the *Arabidopsis thaliana* plant.

Figure S3. Use of image analysis software to estimate the probability of engaging the nanoindenter tip in a desired area near the middle of the cell.

Figure S4. Confocal microscope images of cells of an Arabidopsis leaf stained with fluorescent brightener 28 showing cell boundaries.

Figure S5. Normalized slope versus displacement curves for two of the results obtained from plasmolyzed samples.

Methods S1. Supplemental experimental procedures.

REFERENCES

- Abarca, D., Martin, M. and Sabater, B. (2001) Differential leaf stress responses in young and senescent plants. *Physiol. Plant.* **113**, 409–415.
- Ache, P., Bauer, H., Kollist, H., Al-Rasheid, K.A.S., Lautner, S., Hartung, W. and Hedrich, R. (2010) Stomatal action directly feeds back on leaf turgor: new insights into the regulation of the plant water status from non-invasive pressure probe measurements. *Plant J.* **62**, 1072–1082.
- Allard, F.J., Ambrose, C., Wasteneys, G.O. and Cytrynbaum, E.N. (2010a) A mechanochemical model explains interactions between cortical microtubules in plants. *Biophys. J.* **99**, 1082–1090.
- Allard, F.J., Wasteneys, G.O. and Cytrynbaum, E.N. (2010b) Mechanism of self-organization of cortical microtubules in plants revealed by computation simulations. *Mol. Biol. Cell.* **21**, 278–286.
- Bolduc, J.F., Lewis, L.J., Aubin, C.E. and Geitmann, A. (2006) Finite element analysis of geometrical factors in micro-indentation of pollen tubes. *Biomech. Model. Mechanobiol.* **5**, 227–236.
- Bret-Harte, M.S., Baskin, T.I. and Green, P.B. (1991) Auxin stimulates both deposition and breakdown of material in the pea outer epidermal cell wall, as measured interferometrically. *Planta*, **185**, 462–471.
- Conn, S.J., Gilliam, M., Athman, A., Schreiber, A.W., Baumann, U., Moller, I., Cheng, N.H., Stancombe, A., Hirschi, K.D., Webb, A.A.R., Burton, R., Kaiser, B.N., Tyerman, S.D. and Leigha, R.A. (2011) Cell-specific vacuolar calcium storage mediated by CAX1 regulates apoplastic calcium concentration, gas exchange, and plant productivity in Arabidopsis. *Plant Cell*, **23**, 240–257.
- Cosgrove, D.J. (2005) Growth of the plant cell wall. *Nat. Rev. Mol. Cell Biol.* **6**, 850–861.
- Das, A., Yamada, M.K. and Uchimiya, H. (2010) Programmed cell death in plants. In *Abiotic Stress Adaptation in Plants: Physiological, Molecular and Genomic Foundation* (Pareek, A., Sopory, S.K., Bohnert, H.J. and Govindjee, eds). New York: Springer, pp. 371–383.
- Derbyshire, P., Findlay, K., McCann, M.C. and Roberts, K. (2007) Cell elongation in Arabidopsis hypocotyls involves dynamic changes in cell wall thickness. *J. Exp. Bot.* **58**, 2079–2089.
- Ebenstein, D.M. and Pruitt, L. (2004) Nanoindentation of soft hydrated materials for application to vascular tissues. *J Biomed Mater Res A*, **69A**, 222–232.
- Ebenstein, D.M., Coughlin, D., Chapman, J., Li, C. and Pruitt, L.A. (2008) Nanomechanical properties of calcification, fibrous tissue, and hematoma from atherosclerotic plaques. *J Biomed Mater Res A*, **91A**, 1028–1037.
- Fischer-Cripps, A.C. (2002) *Nanoindentation*. New York: Springer.
- Frommer, J. and Overney, R. (2000) *Interfacial Properties on the Submicron Scale*. Oxford, UK: Oxford University Press, pp. 70–75.
- Goldberg, R., Morvan, C. and Roland, J.C. (1986) Composition, properties and localization of pectins in young and mature cells of the mung bean hypocotyl. *Plant Cell Physiol.* **27**, 417–429.
- Gorshkova, T.A., Mikshina, P.V., Gurjanov, O.P. and Chemiksova, S.B. (2010) Formation of plant cell wall supramolecular structure. *Biochemistry*, **75**, 159–172.
- Green, P.B. and Stanton, F.W. (1967) Turgor pressure: direct nanometric measurement in single cells of *Nitella*. *Science*, **155**, 1675–1676.
- Hamant, O., Meyerowitz, E.M. and Traas, J. (2011) Is cell polarity under mechanical control in plants? *J. Plant Signal Behav.* **6**, 137–139.
- Hayot, C.M., Forouzesh, E., Goel, A., Avramova, Z. and Turner, J.A. (2012) Viscoelastic properties of cell walls of single living plant cells determined by dynamic nanoindentation. *J. Exp. Bot.* **63**, 2525–2540.
- Heisler, M.G., Hamant, O., Krupinski, P., Uyttewaal, P., Ohno, C., Jonsson, H., Traas, J. and Meyerowitz, E.M. (2010) Alignment between PIN1 polarity and microtubule orientation in the shoot apical meristem reveals a tight coupling between morphogenesis and auxin transport. *PLoS Biol.* **8**, 1–12.
- Hoffler, C.E., Guo, X.E., Zysset, P.K. and Goldstein, S.A. (2005) An application of nanoindentation technique to measure bone tissue lamellae properties. *J. Biomech. Eng.* **125**, 1046–1053.
- Inan, G., Zhang, Q., Li, P., Wang, Z., Cao, Z., Zhang, H., Zhang, C., Quist, T. M., Goodwin, S.M., Zhu, J., Shi, H., Damsz, B., Charbaji, T., Gong, Q., Ma, S., Fredricksen, M., Galbraith, D.W., Jenks M.A., Rhodes, D., Hasegawa P.M., Bohnert, H.J., Joly, R.J., Bressan, R.A. and Zhu, J.K. (2004) Salt stress A halophyte and cryophyte Arabidopsis relative model system and its applicability to molecular genetic analyses of growth and development of extremophiles. *Plant Physiol.* **135**, 1718–1737.
- Iwamoto S., Kai, W. and Isogai A., Iwata, T. (2009) Elastic modulus of single cellulose microfibrils from tunicate measured by atomic force microscopy. *Biomacromolecules*, **10**, 2571–2576.
- Johnson, K.L. (1985) *Contact Mechanics*. Cambridge: Cambridge University Press.
- Lintilhac, P.M., Chunfang, W., Tanguany, J.J. and Outwater, J.O. (2000) Ball tonometry: a rapid, nondestructive method for measuring cell turgor pressure in thin-walled plant cells. *J. Plant Growth Regul.* **19**, 90–97.
- Milani, P., Gholamirad, M., Traas, J., Arneodo, A., Boudaoud, A., Argoul, F. and Hamant, O. (2011) *In vivo* analysis of local wall stiffness at the shoot apical meristem in Arabidopsis using atomic force microscopy. *Plant J.* **67**, 1116–1123.
- Mohapatra, P.K., Patra, L., Raval, M.K., Ramaswamy, N.K., Biswal, U.C. and Biswal, B. (2010) Senescence-induced loss in photosynthesis enhances cell wall β -glucosidase activity. *Physiol. Plant.* **138**, 346–355.
- Mokter, H.M.D. and Nonami, H. (2010) Effects of water flow from the xylem on the growth-induced water potential and the growth-effective turgor associated with enlarging tomato fruit. *Environ. Control. Biol.* **48**, 101–106.
- Niklas, K.J. (1992) *Plant Biomechanics: An Engineering Approach to Plant Form and Function*. Chicago, IL: University of Chicago.
- Nobel, P.S., (2005) *Physicochemical and Environmental Plant Physiology*, 3rd edn. Burlington, MA: Elsevier Academic Press.
- Nonami, H. and Boyer, J.S. (1993) Direct demonstration of a growth-induced water potential gradient. *Plant Physiol.* **102**, 13–19.
- Oliver, W.C. and Pharr, G.M. (2004) Measurement of hardness and elastic modulus by instrumented indentation: advances in understanding and refinements to methodology. *J. Mater. Res.* **19**, 3–20.
- Paparozi, E.T. (1981) *The Effects of Simulated Acid Precipitation on Leaves of Betula alleghaniensis, Britt, and Phaseolus vulgaris cv. Red Kidney*. PhD Thesis, Cornell University, Ithaca, New York, pp. 120–133.
- Probine, M.C. and Preston, R.D. (1962) Cell growth and the structure and mechanical properties of the wall in inter-nodal cells of *Nitella opaca* II. Mechanical properties of the walls. *J. Exp. Bot.* **13**, 111–127.
- Routier-Kierzkowska, A.L., Weber, A., Kochova, P., Felekis, D., Nelson, B.J., Kuhlemeier, C. and Smith, R.S. (2012) Cellular force microscopy for *in vivo* measurement of plant tissue mechanics. *Plant Physiol.* **158**, 1514–1522.
- Saha, R. and Nix, W.D. (2002) Effects of the substrate on the determination of thin film mechanical properties by nanoindentation. *Acta Mater.* **50**, 23–38.
- Sancho-Knapik, D., Gómez Álvarez-Arenas, T., Peguero-Pina, J.J. and Gil-Pelegrin, E. (2010) Air-coupled broadband ultrasonic spectroscopy as a new noninvasive and non-contact method for the determination of leaf water status. *J. Exp. Bot.* **61**, 1385–1391.
- Shi, L., Wang, B., Gong, W., Zhang, Y., Zhu, L. and Yang, X. (2011) Actin filaments and microtubules of Arabidopsis suspension cells show different responses to changing turgor pressure. *Biochem. Biophys. Res. Commun.* **405**, 632–637.
- Shibuya, K., Yamada, T., Suzuki, T., Shimizu, K. and Ichimura, K. (2009) In-PSR26, a putative membrane protein, regulates programmed cell death during petal senescence in Japanese morning glory. *Plant Physiol.* **149**, 816–824.
- Somerville, C., Bauer, S., Brininstool, G., Facette, M., Hamann, T., Milne, J., Osborne, E., Paredez, A., Persson, S., Raab, T., Vorwerk, S. and Youngs, H. (2004) Toward a systems approach to understanding plant cell walls. *Science*, **306**, 2206–2211.
- Straatmann, K. (2008) Wound healing assay [WWW document]. URL www.le.ac.uk/biochem/microscopy/pdf/Wound%20healing%20assay.pdf [accessed on 11 October 2012].
- Tricoteaux, A., Duarte, G., Chicot, D., Le Bourhis, E., Bemporad, E. and Lesage, J. (2010) Depth-sensing indentation modeling for determination of elastic modulus of thin films. *Mech. Mater.* **42**, 166–174.
- Tsui, T.Y. and Pharr, G.M. (1999) Substrate effects on nanoindentation mechanical property measurements of soft films on hard substrates. *J. Mater. Res.* **14**, 292–301.

- Wang, C.X., Wang, L. and Thomas, C.R.** (2004) Modeling the mechanical properties of single suspension-cultured tomato cells. *Ann. Bot.* **93**, 443–453.
- Wang, L., Hukin, D., Pritchard, J. and Thomas, C.** (2006) Comparison of plant cell turgor pressure measurement by pressure probe and micromanipulation. *Biotechnol. Lett.* **28**, 1147–1150.
- Wei, C. and Lintilhac, P.M.** (2007) Loss of stability: a new look at the physics of cell wall behavior during plant cell growth. *Plant Physiol.* **145**, 763–772.
- Yuya, P.A., Amborn, E., Beatty, M.W. and Turner, J.A.** (2010) Evaluating anisotropic properties in the porcine temporomandibular joint disk using nanoindentation. *Ann. Biomed. Eng.* **38**, 2428–2437.
- Zhang, C., Halsey, L.E. and Szymanski, D.B.** (2011) The development and geometry of shape change in *Arabidopsis thaliana* cotyledon pavement cells. *BMC Plant Biol.* **11**, 27–40.
- Zhang, Y.F., Bai, S.L., Yang, D.Y., Zhang, Z. and Kao-Walter, S.** (2008) Study on the viscoelastic properties of the epoxy surface by means of nano dynamic mechanical analysis. *J. Polym. Sci. B Polym. Phys.* **46**, 281–288.
- Zhu, L.G. and Boyer, J.S.** (1992) Enlargement in chara studied with a turgor clamp: growth rate is not determined by turgor. *Plant Physiol.* **100**, 2071–2080.
- Zur, B., Boote, K.J. and Jones, J.W.** (1981) Changes in internal water relations and osmotic properties of leaves in maturing soybean plants. *J. Exp. Bot.* **32**, 1181–1191.